Series arc fault location algorithm based on impedance parameters and fault map trace generation

Edwin Calderon-Mendoza, Patrick Schweitzer, Hien Duc Vu, Serge Weber

Series arc fault location algorithm based on impedance parameters and fault map trace generation

Edwin Calderon-Mendoza, Patrick Schweitzer [1], Hien Duc Vu, Serge Weber

University of Lorraine, CNRS, Institut Jean Lamour (IJL), Nancy F-54000, France

ARTICLE INFO

Keywords:
Indoor power line
Fault location
Fault map trace
Series arc fault

ABSTRACT

This paper presents a location algorithm for series arc fault in a low-voltage indoor power line in an AC 230 V 50 Hz home network. At both ends of the line, currents and voltages are recorded for each arc fault generation at different distances. Previously a fault map trace is created by using stored signature coefficients obtained from Kirchhoff equations which allow a virtual decoupling of the line's mutual capacitance. Then, the calculation of signature coefficients using Kirchhoff equations is done by considering hypothetical fault distances where the fault can appear. This procedure allows to obtain a curve with a linear trend. Finally the unknown fault distance is estimated at the intersection of this curve with the fault map trace. In the process of validation of distance estimations, many series arc fault Data (real currents data) that belong to carbonized paths or opening contacts (using copper electrodes) are inserted in the power line. Also, the performance of the algorithm is validated for different line lengths and considering different inductive loads.

Locating series arc faults can be very helpful in the health monitoring of low-voltage power systems in order to efficiently locate the position of damaged cables to avoid electrical fires and save time in restoration of power supply.

1. Introduction

In the home, electrical faults are one of the major causes of fires. A particular problem comes in the form of series-arc faults, that occur when wires become damaged or degraded and are therefore able to come into contact with one another. Another potential cause of electrical fires are loose contacts in connectors. Due to its complex random behavior, this type of fault, in series configuration, is more difficult to be detected because the current level is limited by the load impedance and not for the fault itself, unlike the parallel fault where strong short currents generated can be more easily detected.

Scientific literature presents a wide range of methods for detecting series arc faults. Commercial protection systems, like the AFCI (Arc-Fault Circuit Interrupter), have been successfully deployed in electrical networks to prevent the type of damage which can cause incidents as catastrophic as fires [1–3]. Employing protection systems capable of detecting faults in a line also provides the secondary benefit of reducing the time needed to repair the lines. Despite the existence of various protection systems, no single circuit breaker to date has integrated the possibility of locating series-arc faults that occur during the period when the line is operational. Most commercial devices are based on reflectrometry and require that the power supply be disconnected before they are able to insert signals into the line [4]. An improvement of reflectometry methods to locate faults in the line in operating mode are essentially the STDR and SSTDR methods [5–7]. They are employed to locate intermittent electric arc faults mainly on electrical aircraft wires. However, the impedance matching required between the power line and the load in order to avoid undesirable reflections and also the complexity in designing a special purpose sensor represent the main weaknesses of these methods.

In this context, we address our attention towards algorithms from the literature focused on the high power domain. These algorithms essentially locate parallel faults (linear phase to phase or phase to ground faults and high impedance faults) and they are based on impedance parameters [8–15], methods based on passive reflections [16–19] (traveling wave propagation), methods which use the electromagnetic time reversal [20–22] and methods based on artificial intelligence [23–29] associated in some cases to the Wavelet Packets. These last methods however have the complexity of using ANNs associated with Wavelets which require high frequency rates and they are mainly applied in long transmission lines (up to 300 km or more).

E-mail addresses: edwin-milton.calderon-mendoza@univ-lorraine.fr (E. Calderon-Mendoza), patrick.schweitzer@univ-lorraine.fr (P. Schweitzer), hien-duc.vu@univ-lorraine.fr (H.D. Vu), serge.weber@univ-lorraine.fr (S. Weber).

[1] Jean Lamour Institute in team MAE (Measurements and Electronic Architectures), University of Lorraine, Nancy, France.

https://doi.org/10.1016/j.ijepes.2020.106652

Nomenclature

$[I(x)]$	Signature vector
$[Q(x)]$	Fault map trace
ω	Angular frequency
C	Capacitance per meter of the line length
d	line length
$DFFT$	Discrete Fast Fourier Transform
G	Conductance per meter of the line length
$I_1^{'}(f)$	DFFT of estimated current on the input side of the arc fault
$I_1^{'}(t)$	Estimated current on the input side of the arc fault
$I_2^{'}(f)$	DFFT of estimated current on the outgoing side of the arc fault
$I_2^{'}(t)$	Estimated current on the outgoing side of the arc fault
$I1_{50Hz}^{'}$	Fundamental harmonic on the input side of the arc fault
$I2_{50Hz}^{'}$	Fundamental harmonic on the outgoing side of the arc fault
I^{+}	Positive current threshold
I^{-}	Negative current threshold
$I_1(f)$	DFFT of the measured current delivered by the supply voltage
$I_1(t)$	Measured current delivered by the supply voltage
I_{1nc}	Estimated current on the input side of the arc fault (virtual decoupling case)
$I_{1nc}(f)$	DFFT of estimated current on the input side of the arc fault (virtual decoupling case)
$I_{1nc50Hz}$	Fundamental harmonic on the input side of the arc fault (virtual decoupling)
$I_2(f)$	DFFT of the measured load current
$I_2(t)$	Measured load current
I_{2nc}	Estimated current on the outgoing side of the arc fault (virtual decoupling case)
$I_{2nc}(f)$	DFFT of estimated current on the outgoing side of the arc fault (virtual decoupling case)
$I_{2nc50Hz}$	Fundamental harmonic on the outgoing side of the arc fault (virtual decoupling)
I_{c_1}	Capacitance current in first section of the line (virtual decoupling case)
I_{c_2}	Capacitance current in second section of the line (virtual decoupling case)
L	Inductance per meter of the line length
L_L	Load inductance
P_1	Cooling power according to Mayr
P_2	Cooling power according to Ayrton
R	Resistance per meter of the line length
R_L	Load resistance
t_C	Time constant
$V_1^{'}(f)$	DFFT of the estimated voltage on the input side of the arc fault
$V_1^{'}(t)$	Estimated voltage on the input side of the arc fault
$V_2^{'}(f)$	DFFT of the estimated voltage on the outgoing side of the arc fault
$V_2^{'}(t)$	Estimated voltage on the outgoing side of the arc fault
$V_1(f)$	DFFT of the measured voltage delivered by the supply voltage
$V_1(t)$	Measured voltage delivered by the supply voltage
$V_2(f)$	DFFT of the measured load voltage
$V_2(t)$	Measured load voltage
V_o	Arc voltage constant
x	Distance of the arcing fault
Z_C	Corona resistance
Z_M	Circuit resistance
Z_p	Impedance that results from G//C

Little work has been devoted to locate faults on low voltage lines of short length (up to 200 m). In literature, some authors presented location methods using the impedance of the electric line [30,31] or Wavelets features which allow to train an ANN [32].

The series arc-fault location methods for short low voltage lines involve challenges since conventional mesh Kirchhoff equations used to locate parallel faults can not be used directly as it is impossible to split the line into two parts on either side of the arc fault. Indeed, a series arc fault behavior is quite similar to an impedance with stochastic variations.

Series arc-fault location methods for DC low voltage power lines are based in the time shift between parallel capacitors current pulses at both ends of a short power line (up 300 m long line) [33–35] or on a parameter impedance model of a 1200 meter emulated transmission line [36]. Both of these methods are interesting; however, the first method seems very sensitive to the noise and eventually has no potential application to AC power lines (short-circuit produced by the insertion of parallel capacitors at the 50 Hz current frequency). In addition, this method requires a very precise synchronization of the measured currents unlike the second method which remains simple with a low computational burden.

On this basis, inspirited by this second method, the authors of this paper developed two original algorithms to locate AC series-arc faults. The first based on an approach model of a home electrical line [37] and the second uses impedance parameters of the line and a neural network [38]. Nevertheless, the accuracy of these methods is strongly influenced by both an adequate frequency band selection or the dynamic variations of different series-arc faults (random and stochastic impedance behavior) which cause significant degradation in their performances. Within this framework, the main focus of this work is on:

– series-arc faults location,
– arcing fault location on short power lines,
– development of a method that operates continuously without the necessity to disconnect the load or supply voltage. The main applications concern health monitoring of low-voltage power systems.

In the present work, we propose a more robust fault location method based on a fault map trace created by using signature coefficients obtained from Kirchhoff equations which allow a virtual decoupling of the line's mutual capacitance. Then, the calculation of signature coefficients using Kirchhoff equations is done by considering hypothetical fault distances where the fault can appear. This procedure allows to obtain a curve with a linear trend. Finally the unknown fault distance is estimated at the intersection of this curve with the fault map trace. The method is tested using different line lengths (from 30 m to 200 m) supplied by a 230 V - 50 Hz source using different series arc faults data and also considering the presence of inductive loads.

2. Short power line model

An electric line with a total length of 'd', containing a series-arc fault located at a distance from the power source referred to as 'x', can be modeled using the T equivalent circuit model of the transmission line according to the diagram displayed in Fig. 1. The line impedance parameters are given in Table 1. Voltages and currents are recorded at points along both ends of the line. This line is described by using its line parameters: R, L, C and G. The line is powered by a 230 V - 50 Hz source and the load is initially composed of a $R_L = 47Ohms$ ($L_L = 0$).

The part of the line lying in front of the fault can be entirely modeled using an equivalent circuit that consists of a series impedance ($R * x$ in

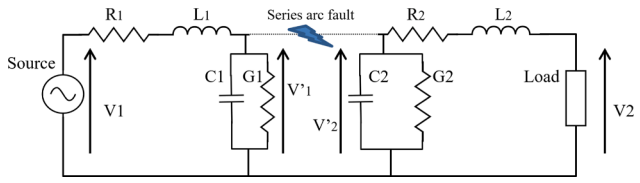

Fig. 1. An electrical model of the faulty power line.

Table 1
Line impedance parameters.

Source	R	L	G	C	Frequency	Load
220 V	$R_1 = R.$ x $R_2 =$ R(d-x)	$L_1 = j\omega L.$ x $L_2 =$ $j\omega L(d\text{-}x)$	$G_1 = G.$ x $G_2 =$ G(d-x)	$C_1 = C.$ x $C_2 =$ C(d-x)	50 Hz	$R_L =$ 470Ω ($L_L = 0$)

series with $L * x$) and a shunt impedance ($G * x$ in parallel with $C * x$).

The second section of the line, found between the point where the fault occurs and the load, will include $R * (d - x)$ in series with $L * (d - x)$ and a parallel conductance $G * (d - x)$ with a capacitance $C * (d - x)$) that is connected to the ground.

An LCR meter (HP 4263A) is used on a 1-meter section of the cable in order to estimate the parameters of the line. Thus, the measured values used in the model are:

$R = 15.9643 * 10^{-3}\ \Omega$;
$L = 0.00069592 * 10^{-3}$ H;
$G = 17 * 10^{-10}$ S;
$C = 5.74 * 10^{-11}$ F.

In the case of the arc fault, it is not possible to create a simple model of impedance that can be inserted into the line model. As this type of defect is highly chaotic, its behavior is very difficult to model. For this reason, an experimental test bench can be employed, as it is capable of reproducing the type of arc fault whose signature can be inserted into the power line model.

3. Series arcing fault

The line current signature required for the location method can be obtained by using either an arc fault model or experimental measurements for the fault. The purpose of this part is to choose which of these two solutions is the most adapted to our problem.

Many authors have already proposed electrical models of arc faults [39,40]. The arc fault model (widely used for series arc fault detection purposes in home electrical networks) presented in Fig. 2 was developed and described in previous studies [41].

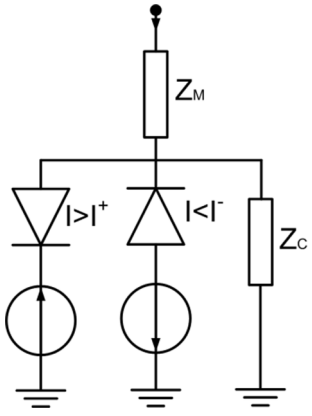

Fig. 2. The arc fault model.

In this model, the diodes are considered as current diodes whose threshold is a current of low value and represents the transition between the corona and the arc discharge phenomena.

The diodes in question are considered to be current diodes, whose threshold is a low-value current. This low-value threshold represents the transition between the corona and the arc-discharge phenomena. This model also includes a time-fixed impedance Z_C, that only occurs at the point where the arc current attains a value between I^+ and I^-.The main parameters values, that were used during the modeling of the arc fault, are provided in Table 2.

The model presented in [13] includes a time-varying series resistance which allows a better representation of the fault. However, the time-varying behavior was approximated by a polynomial function which was adjusted through field test of real fault case of parallel faults on a 230 kV transmission line. This fault (line to ground) depends on specific characteristic of the contact surface of faulted point, such as porosity, humidity, density and composition of the soil. Therefore, this model is more suitable for describing parallel arc faults on high power lines.

In practice, the process of initiating an experimental series-arc can be accomplished through the use of either carbonized paths or opening contacts (in accordance with the UL 1699 standard), as seen in (Fig. 3). The opening-contact test was carried out using two 6 mm-diameter copper electrodes. In the case of the carbonized path (generated using a high-voltage generator) a single cut was made to the insulating material of 2 parallel sections of wire, which were then joined together. Fig. 3 shows the experimental test configuration that was developed in order to obtain the line-current data. The power source (230 VAC - 50 Hz) supplies a load (Resistive/Inductive). The arc fault, that is produced in a chamber where the temperature and pressure can be controlled, is inserted in series, into the power line.

All measurements are taken using a Lecroy Pro 950 oscilloscope (2 GHz bandwidth) and the AP015 current probe (75 MHz bandwidth) at a sampling rate of 1 MHz.

When a series-arc fault is produced using the experimental test bench (for a duration of approximately 0.5 s), the current that is registered is intrinsically related to the real parameters of the line. It can therefore be perfectly inserted into the indoor-power-line model. By following this procedure, we are able to overcome the problem of being forced to use a series-arc-fault model that does not consider the dynamic variations of the parameters present in the case of a real arc fault.

Fig. 4 shows the evolution over time, of the line-current signatures that were obtained through measurement and simulation (taking into account models from [39,40]). The electric arc is a naturally chaotic phenomenon and it is highly affected by environmental conditions (temperature, humidity and pressure for example) and the parameters of the power line (its length, the appliance it is attached to, etc.).

The maximum amplitude levels of the line current vary from one alternation to another and the impedance of the arc changes over time. The wave form also has a phase-shift that gradually varies. In a similar fashion, results show that ignition voltages also vary over time. It is therefore difficult to model it's evolution precisely, due to the chaotic nature of arcing faults.

For all of these various reasons, we have opted to work with a

Table 2
The parameters of the arc fault model.

Symbol	Value	
V_0	30	V
P_1	2000	W
P_2	2	W
I+	0,0035	A
I−	−0,0035	A
Z_C	10000	W
Z_M	285	W
t_C	0,00053	s

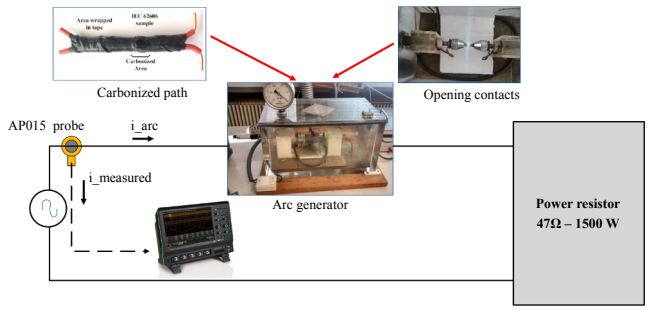

Fig. 3. The experimental test bench.

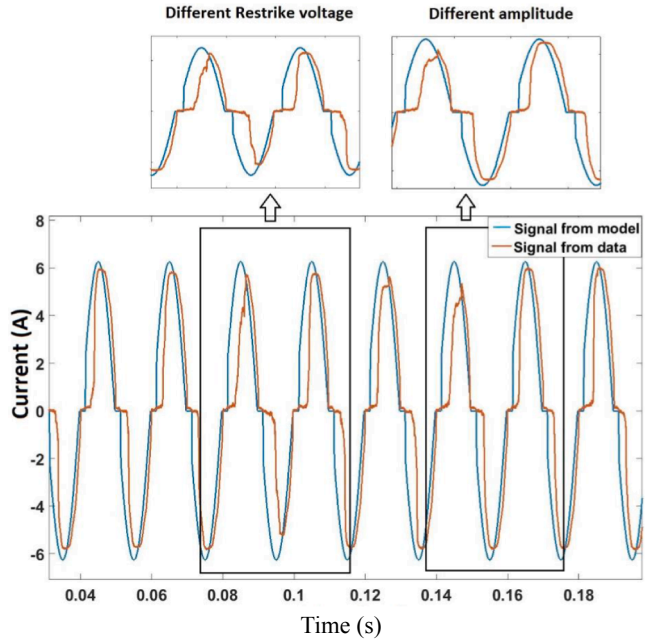

Fig. 4. A comparison of series arc fault currents.

genuine arc current. It is measured when the arc fault is initiated and then inserted into power-line models used for validation.

The arc current can be directly inserted into the electrical circuit via a Simulink box which acts as a 'controlled-current' source (see the selected part noted Measured Data in Fig. 5). This device is analogous to the variable impedance that limits the current flow across the line. It consequently induces behavior (such as the variation of random impedance in the power line) similar to that witnessed in the event of a real series-arc fault.

4. Influence of the mutual capacitance in the power line

In the general scheme of the transmission line given in Fig. 1, an electrical arc fault occurs at a distance noted 'x' meter from the electrical source (total line length of d meters).

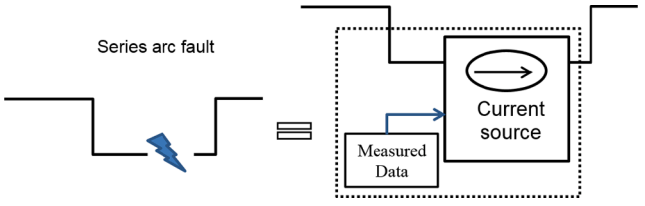

Fig. 5. Data injection by using a controlled current source.

From the line currents and voltages, the equations of the two meshes in the frequency domain can be written in the following equations:

$$V_1^{'}(f) = V_1(f) - (R * x + j\omega * L * x) * I_1(f) \quad (1)$$

$$I_1^{'}(f) = I_1(f) - V_1^{'}(f) * (j\omega * Z_p * x) \quad (2)$$

$$V_2^{'}(f) = V_2(f) + (R * y + j\omega * L * (d - x)) * I_2(f) \quad (3)$$

$$I_2^{'}(f) = I_2(f) + V_2^{'}(f) * j\omega * Z_p * (d - x) \quad (4)$$

In these equations Z_p represents the impedance that results from the parallel association of G and C.

Eqs. (2) and (4) are highly dependent on Eqs. (1) and (3). These equations obtained make it possible to establish mathematical relationships at the input and output of a series arc fault (Fig. 6) inserted in an unknown section of the power line.

From the displayed Fig. 6, two rules can be deducted. First: $I_1^{'} - I_2^{'} \approx 0$ and the second: $V_1^{'} - V_2^{'} > 0$. For a more precise approach to a fault distance, we choose the current difference. The principle of the location method is based on the estimation of the current flowing through the arcing fault. In practice, since the current flowing at the input and at the output of the fault impedance is the same, this condition is obtained for the exact value of the fault distance. The idea is therefore to increment the distance x until reaching a minimum for $I_1^{'} - I_2^{'}$. The fault distance will be the one replaced in the equations described above which allow to obtain the minimum trend.

4.1. Case of a simplified line model

In this scenario, Zp is considered to equal G. This means that the parallel mutual capacitance is not taken into account. As is the case in a line of short length (<100 m), the influence of C is weak and can be neglected. It's value is close to 0. A complete diagram of the simplified power-line model, that displays both the line sections and the arc fault, is shown in Fig. 7.

Using this model, an estimation of the fault distance is carried out according to the steps:

– Step 1: The voltages at both ends of the line V1(t) and V2(t), as well as the associated currents I1(t) and I2(t), are measured when a fault is present in the circuit.
– Step 2: The Discrete Fourier Transform is used to calculate the electrical quantities $I_1(f) = DFFT[I1(t)], I_2(f) = DFFT[I2(t)], V_1(f) = DFFT[V1(t)]$ and $V_2(f) = DFFT[V2(t)]$.
– Step 3: The values of I1′(f) and I2′(f) are then calculated using Eqs. (1)–(4).

Note: In the proposed method, analysis is done at 50 Hz (the frequency of the European Electricity Network). At this frequency, the fault distance influence on the current and voltage is preponderant. In addition, fundamental harmonics are not influenced by the electromagnetic noisy or parasitic currents which are originated by series-arc faults. The calculation is thus limited to the evaluation of

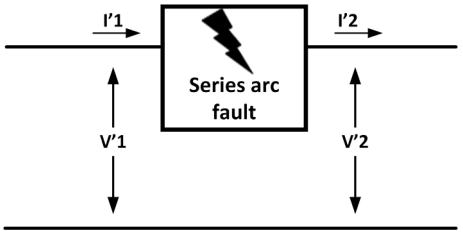

Fig. 6. Series arc fault with input–output relationships.

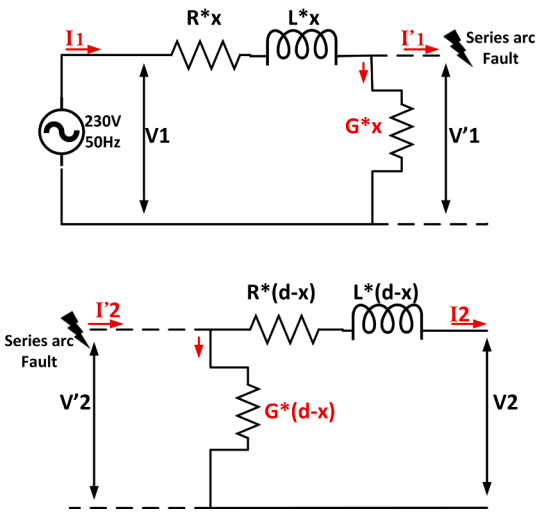

Fig. 7. A simplified model of an indoor power line.

the two following quantities: $I1'_{50Hz} = max(abs(I1'(f))$ and $I2'_{50Hz} = max(abs(I2'(f))$.

- Step 4: For all hypothetical fault distance values, steeped faults from 1 meter to $(d-1)$ meter (in step of 1 meter) are considered in the calculation of the absolute value of the difference $I1'_{50Hz} - I2'_{50Hz}$. Then, these coefficients obtained (named signature vector) versus their associated distances are plotted.
- Step 5: The estimation of the fault distance is obtained by searching for the particular distance in the range [1, 2, ... $(d-1)$] for which ABS $(I1'_{50Hz} - I2'_{50Hz}) = 0$.

The proposed method of detection is tested on a power line of 60 meters in length. Two series arc faults are ignitiated, the first at 20 meters (example1) and the second at 40 meters (example 2) from the source. The fault distance are assumed to be unknown for the purpose of the tests.

The procedure given above (from Step 1 to 5) is followed to estimate the distance. For Step 4, the evolution of ABS $(I1'_{50Hz} - I2'_{50Hz})$ are represented in Figs. 8 and 9 for each distance in the interval 1–59 m. According to Step 5, only one point in Figs. 8 and 9. match the condition of perfect intersection with the abscissa axis, with ABS $(I1'_{50Hz} - I2'_{50Hz}) = 0$. Then, the particular distances of 10 m and 40 m satisfy the condition required. Thus, these estimated fault distances correspond perfectly to the real fault distances.

Nevertheless, the parallel capacitance in the model of the transmission line must be taken into account and can not be neglected. Thus, Kirchoff equations are applied considering G//C equals Zp. The algorithm is then tested taking into account series arc faults at distances of 10 m, 20 m, 30 m and 40 m. The results are displayed in Fig. 10.

We can observe that the effect of mutual capacitance is detrimental to the algorithm. The adverse effects are produced by the unbalance of

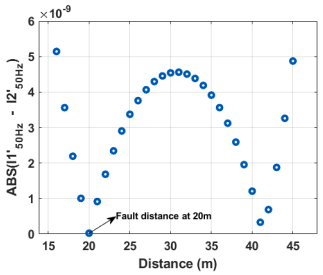

Fig. 8. Fault distance estimation example 1 (considering C = 0).

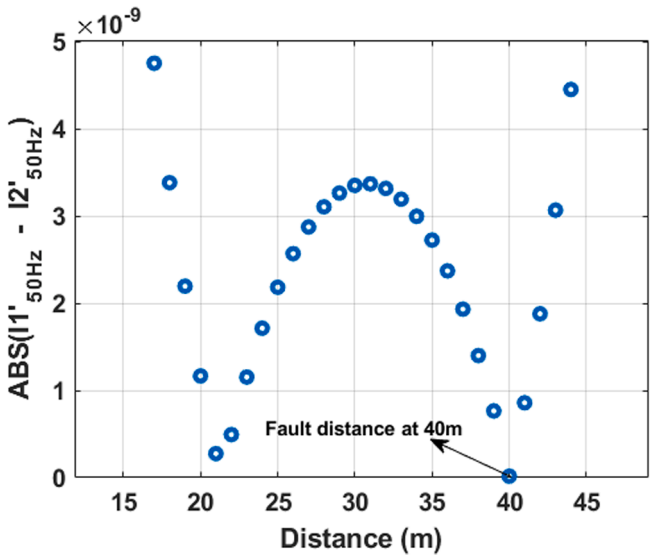

Fig. 9. Fault distance estimation example 2 (considering C = 0).

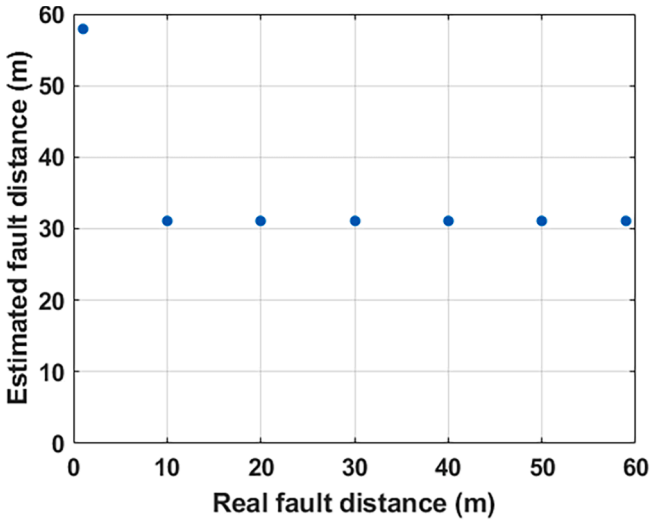

Fig. 10. Fault distance estimations (considering that C ≠ 0).

Kirchhof equations which does not allow the correct estimation of fault distances. We can notice the presence of offsets in the calculation of coefficients $I1'_{50Hz} - I2'_{50Hz}$. Thus, it appears clearly that the condition $I1'_{50Hz} - I2'_{50Hz} = 0$ is never fulfilled for none of the fault distances. These characteristics are shown in Fig. 10 where the coefficient the closest to zero taken by the algorithm is the one that belongs in most cases (exept for the fault at 1 m) to the estimated fault distance of 31 m (wrong estimation).

4.2. The mutual capacitance decoupling

The limits of this fault-location method are noticeably linked to effect of mutual capacitance. For this reason, we have decided to develop an original approach based on the virtual decoupling of mutual capacitance. By taking this assumption into account, we can calculate fault currents with virtual decoupled capacitance effects at both sides of the series arc fault.

Considering the strong influence of the parallel capacitance between two cables, we voluntary decided in this part to neglect the parallel conductance (G = 0) for its weak influence in the power line. Thus, Zp is

made up of a parallel capacitance whose intensity depends on the fault distance.

The simplified Kirchhoff equations for determining fault currents with a virtual decoupled capacitance at the input and output of a series arc fault can be obtained from Fig. 11.

If we consider the part of the line found on the left-hand side, the estimation of the current is obtained using the equation: $I_{1nc} = I_1 - I_{c_1}$. In this case, the physical influence of the mutual capacitance, contained in the measured current, is virtually decoupled using: $I_{c_1} = j\omega C * x(V_1(f) - (R * x + j\omega L * x)I_1(f))$. Similarly, from the chunk of the line found on the right-hand side, a current with no capacitive influence is obtained from: $I_{2nc} = I_2 + I_{c_2}$. Here, the virtual decoupling (in accordance with the functioning of the power-line model) is accomplished by adding $I_{c_2} = j\omega C * y(V_2(f) + (R * y + j\omega L * y)I_2(f))$. The resulting equations, that are applied to both the left and right sections of the line are therefore presented as follows:

$$I_{1nc}(f) = I_1(f) - j\omega C * x(V_1(f) - (R * x + j\omega L * x)I_1(f)) \quad (5)$$

$$I_{2nc}(f) = I_2(f) + j\omega C * y(V_2(f) + (R * y + j\omega L * y)I_2(f)) \quad (6)$$

The equations presented above, depend on the unknown fault distance 'x', and they can be used at first to create a fault map-trace which is composed of a set of feature coefficients. These coefficients can be obtained at different arc-fault positions along the length of the line. Thus, a model of series arc fault developed by Lezama [39] is inserted at particular points of the line. It allows us to visualize the evolution of the series-arc fault at a range of different distances. It also represents a baseline, from which we can make estimations of fault distances.

5. Fault map construction and fault location algorithm

5.1. Fault map trace

The electric line of length d that we are studying is characterized by its own signature $[Q(x)]$. For this we consider that the electric arc fault may appear for distance (x = 1 m, x = 2 m, …..x = d-1 m). The procedure to build $[Q(x)]$ from the modeled faulty line (see Fig. 1) for our 200 meter long line is as follows:

From the electrical T model of the electric line, the arc fault model is inserted at different positions across the line. For each arc fault test carried out at a specific distance, currents and voltages are recorded at both ends of the line. The coefficients $I_{1nc50Hz}$ and $I_{2nc50Hz}$ at the fundamental frequency are calculated according to Eqs. (5) and (6). The next step is to obtain a calculation of coefficients using the equation $I_{1nc50Hz} - I_{2nc50Hz}$ versus their corresponding real fault distances. A map trace for a power line of 200 m in length is displayed in Fig. 12.

An estimation of the current, that takes into account the virtual decoupling, allows us to confirm the trend $I_{1nc50Hz} - I_{2nc50Hz} \approx 0$.

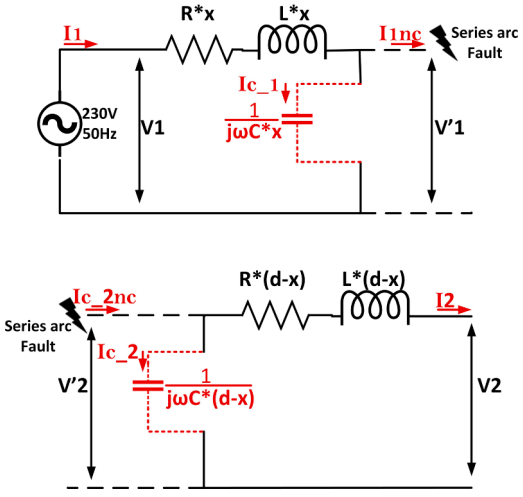

Fig. 11. The virtual decoupling of the power line.

5.2. Fault location algorithm

The fundamental part of the fault location algorithm is based on iterative calculations of the subtraction $I_{1nc50Hz} - I_{2nc50Hz}$. This takes into account hypothetical stepped fault distances values which are replaced in the Kirchhoff Eqs. (5) and (6). Fig. 13 presents a diagram that describes the algorithm.

The first step in the procedure, is to calculate the DFFT of the recorded signals: I1, V1, I2 and V2. They are later substituted in the Kirchhoff equations through a process of analyzing the initial fault distance (x = 1 m). The fundamental harmonics of the estimated currents are then extracted in order to find the difference: $I_{1nc50Hz} - I_{2nc50Hz}$. Both this value, and the value of 'x', are stored by means of an incremental array.

We will thus continue the process for all of the distances referred to as 'x' (x = 2 m, 3 m, 4 m, etc., until the point we reach d-1 m). After working on $d-1$ iterations, the array $[x\ I(x)]$ is completed. The signature vector $[I(x)]$ that we obtain is compared with the fault-map trace vector $[Q(x)]$ that is already stored. The final step is to estimate the fault distance by searching for the intersection $[I(x)] \cap [Q(x)]$.

The fault map trace obtained in the previous subsection, through the use of the dynamic of a series arc fault model, is only stored once. It will be used without making any changes on the value of its coefficients, even during the different stages of validation (as we will show in the next section).

6. Results

In this section, we have selected three different configurations of the distribution line to test the validity of our method. Thus, a lumped line model, a π line model and a distributed line model displayed in Fig. 14 have been tested for validation of our series arc fault location algorithm.

The accuracy of the proposed algorithm, is validated by the use of current data sets obtained from the generation of arc faults during the process of various experiments which have been carried out using the experimental test bench (carbonized-path and opening-contact tests).

For the three configuration of power lines used for validation, experimental current fault data were inserted according the process in Fig. 5.

The validation of the method using is constituted by a simplified line model without parallel capacity (line represented in Fig. 14a. Therefore, the estimation of series arc fault locations can be performed using Eqs. (1)–(4). Data 1 (opening contacts) is inserted in the line. The results

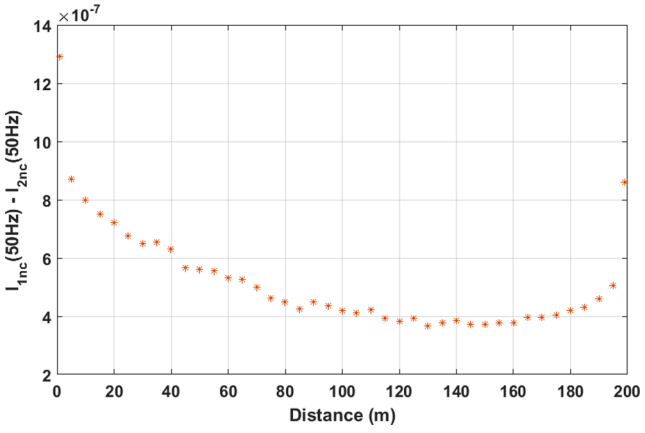

Fig. 12. Fault map trace for a line of 200 m.

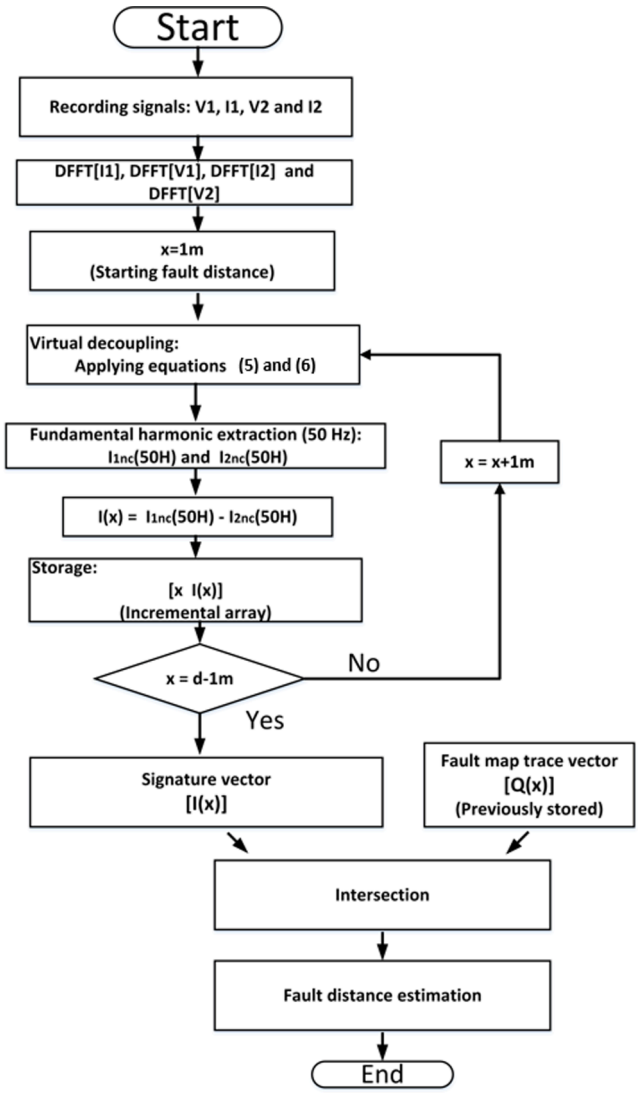

Fig. 13. Algorithm for locating series arc fault (capacitance decoupling).

show that the fault distance is accurately estimated for 99% of cases.

More exhaustive validation steps are carried out for configurations of Fig. 14b and c which have included parallel capacities. Thus, the estimate of series arc fault positions is determined using Eqs. (5), (6) and $[Q(x)]$. Since the results obtained for the two configurations are very similar, the validation of the method for the configurations π and the distributed lines is defined by the following steps:

The first step in the process of validation, is to generate data regarding the positions of the series-arc faults along the length of the power line, at points: 5 m, 110 m and 180 m (The the results are displayed in Fig. 15). Data 1 (the opening contacts), as well as Data 2 and Data 3 (the carbonized paths), are used respectively. The resulting estimations of distance are displayed in Fig. 15.

It can be observed that the algorithm is able to locate fault distances with a very high level of accuracy (for estimations made at points: 5 m, 109 m and 110 m) with a very good accuracy. The signature vectors $[I(x)]$ obtained for each fault distance are intersected with the fault map trace. If we examine the example of the fault produced at 5 m, we can observe that the coefficient obtained from $I_{1nc50Hz} - I_{2nc50Hz}$ (for the iteration that occurs at 5 m, which is the supposed fault distance) is very close to the type of coefficient that best corresponds to the real fault distance. Similarly, in the case of other estimations of fault distance, we are able to observe that the signature coefficients fit well with the type coefficients of the fault map trace, that correspond to real fault

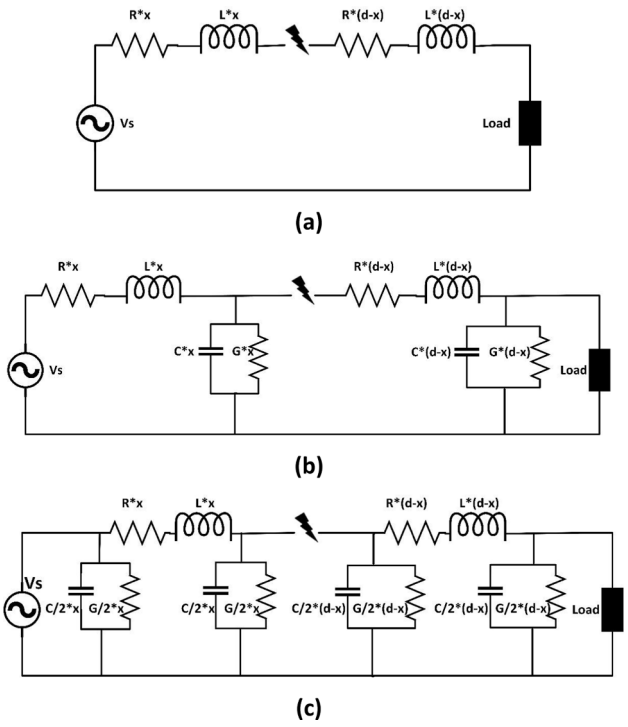

Fig. 14. Line models for validation. (a) Lumped line model. (b) Distributed line model. (c) π line model.

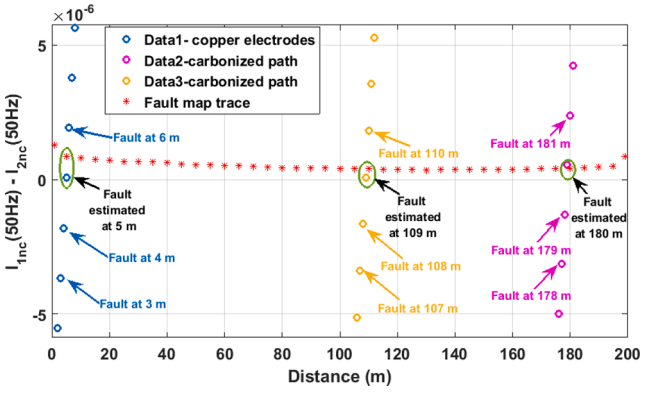

Fig. 15. Estimations of distances for different arc fault dynamics.

distances.

In order to confirm that our aims are justified, the algorithm must also tested using complementary Data sets obtained from different tests.

Indeed, the electric arc has a highly random behaviour as shown in Fig. 4 and thus the line current signature will be different from one electric arc to another. A location measurement result obtained with a single arc recording does not allow the location method to be generalized. To do this, Data4 - Data5 - Data6 and Data7 are the measurements obtained by considering different opening contact tests are additional measurements and inserted into the power line.

Data8, Data9, Data10 and Data11 (obtained from experimentation with carbonized paths) are also used in the validation process.

In order to quantify the discrepancy between the real fault distances and the respective estimations of their measurements, The errors related to each real fault distances are calculated using Eq. (7). The results of errors in estimating fault distances are presented in both Figs. 16 and 17.

$$error = \frac{estimated\ fault\ distance - real\ fault\ distance}{line\ length} \tag{7}$$

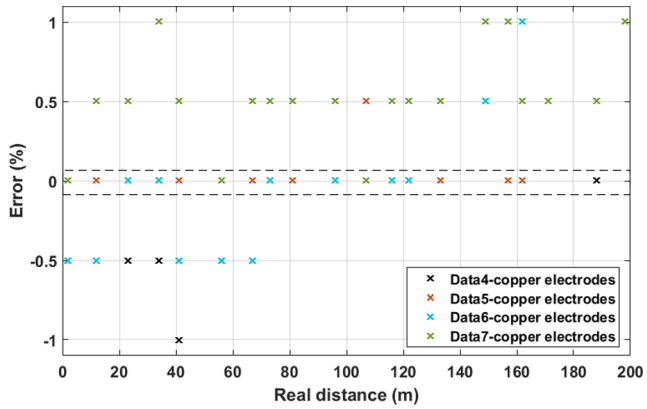

Fig. 16. A chart of the errors obtained to different arc fault data from the opening contacts test.

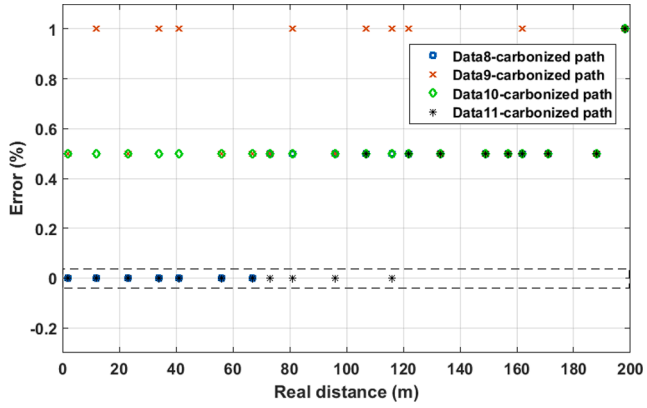

Fig. 17. A chart of the errors related to different arc fault test from the carbonized path.

During this stage of validation, the rate of error is at a level between 0% and 1% for all of the data sets. For the opening contacts test, the algorithm perfectly estimates the fault distances (majority of points for an error = 0). For the carbonized path test, the location method is a little less efficient although the estimated fault distances are close to the real ones (for which error = 0.5 for a majority of points).

It should be noted that the dynamic of different arc faults does not have a significant influence on the algorithm (for either the opening contacts or the carbonized paths).

The second step in the validation process is to test the algorithm at different lengths along the power line but, this time, using the same stored fault-map trace (in this case, a fault-map trace for a power line of 200 meters in length). The algorithm is thus tested using a range of different line lengths, from 30–190 meters. The series-arc fault, that is inserted into the power lines, belongs to Data 12 (taken from the opening-contacts test). The results obtained from this test are presented in Table 3.

We find that the estimations of the fault distances, made at different line lengths, are very close to the real fault distances. The estimations shown in orange, represent the variations of the measurements of up to a length of 2 meters, in respect to the real fault distances. We are able to make very accurate estimations for the line lengths of 30, 50 and 70 meters, if we take the results we have obtained into account. At the line lengths of 80–190 meters however, the quality of the estimation is somewhat diminished (mainly at fault distances that are found close to the load). Given this information, a maximum erroneous measurement of 5 m will be observed in the case of a fault produced at 189 m (an estimation of 184 m), when we are testing a line of 190 meters in length.

Table 3
Fault distance estimations for different line lengths.

Line	Fault distance (m)																												
length	3	8	13	20	27	33	40	49	52	59	67	74	79	89	91	98	109	119	128	133	138	148	159	168	178	189			
30 m	3	8	13	20	26	–	–	–	–	–	–	–	–	–	–	–	–	–	–	–	–	–	–	–	–	–			
50 m	3	8	13	20	27	32	40	48	–	–	–	–	–	–	–	–	–	–	–	–	–	–	–	–	–	–			
60 m	3	8	13	20	27	33	40	48	52	56	–	–	–	–	–	–	–	–	–	–	–	–	–	–	–	–			
70 m	3	8	13	19	26	33	40	48	52	58	66	–	–	–	–	–	–	–	–	–	–	–	–	–	–	–			
80 m	3	8	13	20	26	33	40	49	52	59	67	73	75	–	–	–	–	–	–	–	–	–	–	–	–	–			
90 m	3	8	13	19	26	33	40	49	52	59	67	73	78	85	–	–	–	–	–	–	–	–	–	–	–	–			
100 m	3	8	13	20	26	33	40	49	52	59	67	74	78	86	90	96	–	–	–	–	–	–	–	–	–	–			
120 m	3	8	13	20	26	33	40	49	52	59	67	74	78	86	90	98	108	115	–	–	–	–	–	–	–	–			
150 m	4	9	13	20	26	33	40	49	52	59	67	74	78	86	90	98	109	118	126	132	136	144	–	–	–	–			
170 m	4	9	14	20	27	33	40	49	53	59	67	74	79	87	90	98	109	118	126	132	136	146	157	165	–	–			
190 m	4	9	14	20	27	33	40	49	53	59	67	74	79	87	90	98	109	118	126	132	136	146	157	166	176	184			

During the third stage of the validation process, the algorithm is tested using different inductive loads. The inductances that are used range from $1mH \leqslant L_L \leqslant 50mH$. The resistive part is maintained at a level of $R_L = 47\Omega$.The currents of Data 13 (derived from the carbonized-path arc-fault tests) are inserted into a power line of 200 m in length. The resulting estimations of fault distances are summarized in Table 4.

In the case of $L_L = 1mH$, the estimations of fault distances are very accurate. The estimated values, shown in green, do display a variation level with a maximum measurement of up to 4 m, in respect to real fault distances however. Despite this, we can still consider them to be sufficiently accurate for our purposes. The accuracy level of the estimations made using $L_L = 50mH$ is noticeably less precise however. This is due to the fact that the coefficients of the signature vector $[I(x)]$ create a displacement that causes them to move away from the fault-map trace. The type of intersections that we are seeking to locate, and that correspond to the fault estimations, are therefore affected.

In the fourth validation step, the algorithm is tested under parallel capacitance variations of π and distributed line models. This, saving the capacitance value obtained in Section II. Thus, we perform the algorithm in cases where the capacitance of the lines does not correspond to the capacitance of the model employed by the fault location algorithm.

In this validation step, we limited maximum variations of the capacitance in the range from −50% to +50% of its nominal value. The results are presented in Table 5.

The estimates of fault location obtained are directly linked with capacitance variations in the configuration lines used for validation (π and distributed models). On one hand, a capacitance variation of −50% in the lines, involve estimates of the location of the faults to 50% below real fault positions. On the other hand, a variation of capacitance of +50% in the lines, implies estimates of fault location 50% above real fault positions.

The final step of the validation imply the modification of all the lines' parameters (Fig. 14a and b) that are $R = 17.5 * 10^{-3}$ ohms, $L = 0.00049 * 10^{-3}$ Henry, $G = 27 * 10^{-10}$ Siemens, and $C = 7.7 * 10^{-11}$ Farad.

The impedance parameters used by Eqs. (5) and (6), are kept in line with the values shown in Section II. During this stage of validation, series arc faults are inserted along a line of 70 meters in length using Data 14 (opening contact). series arc faults that use Data 15 (carbonized path) are inserted to different positions along a 40 meter line. The subsequent results obtained are displayed in Fig. 18

In the case of the 70-meter line, the level of estimation errors rises in a linear fashion, as the arc-fault position increases (the measurement of the distance uses the source as a reference). The highest rate of error corresponds with the fault located at a point of 70 m, where it can reach up to 33%. In a similar manner, errors that were recorded, when testing a line of 40 meters in length, display a linear trend. A maximum level of error of 20% occurs at a distance of 30 meters however.

During this final stage of validation, we are able to confirm also that the performance of this method can be affected by the estimations of the parameters of the line, that are used by the algorithm. Despite this being the case, the results obtained during our tests, show only moderate levels of error and the manner in which real fault distances are tracked can be considered to be acceptable.

Table 5
Capacitance variation (in the case of a 200 m length line).

Capacitance variation	Real fault distance position					
	10 m	30 m	70 m	120 m	160 m	199 m
$C = 2.87*10^{-11}$ (−50% variation)	5 m	15 m	35 m	60 m	80 m	98 m
$C = 8.61*10^{-11}$ (+50% variation)	15 m	45 m	105 m	180 m	–	–

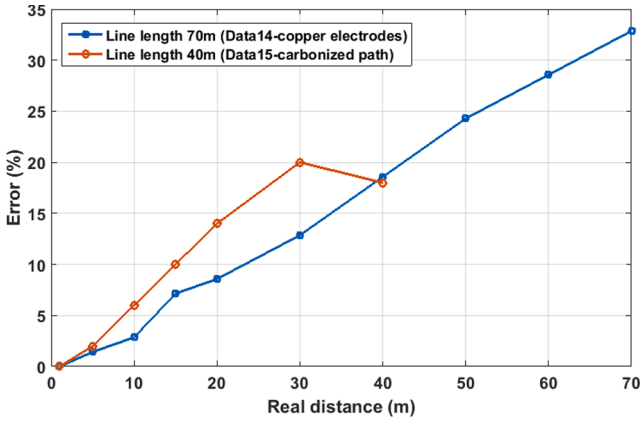

Fig. 18. The estimation of errors for different line's parameters.

The obtained results with the proposed method of arcing fault location in low length electric lines have been compared with different methods from literature. In Table 5, we present the summary of all the methods in low voltage lines including the method proposed in this paper. Electrical line lengths are comprised between 25 and 1200 meters. First of all it is important to specify that few methods concern the location on lines of short length. Three of the methods are dedicated to the DC domain and the three others to AC applications. From Table 6, most of the methods are based on the analysis of the impedance parameters associated for two of them with artificial intelligence (genetic algorithm and neural network). Table 5 shows that most of the methods have been tested with resistive loads, unlike our method also tested with inductive loads. The method presented in [33], based on travelling waves, has a good accuracy but requires very high synchronisation. As for the method presented in [28], it concerns parallel intermittent faults which can be closed to short circuit faults.

One considerable advantage is that our method is less sensitive to series arc fault impedance variations, that can be quite important with arcing faults. On the same, in terms of error, our method is quite performing (Error = 1%). As most of the other method require the selection of a frequency band of analysis, in our case, the analysis is done at 50 Hz.

Table 4
The estimations of fault distances, considering different inductance values (in the case of a 200 m length line).

Load	Fault distance (m)									
inductance	5	18	33	53	67	100	120	165	173	189
1 mH	5	18	33	53	67	100	120	165	173	189
5 mH	4	17	32	52	66	99	119	168	177	188
10 mH	5	23	40	61	76	99	118	167	175	188
20 mH	11	24	39	57	69	100	120	165	177	186
30 mH	10	22	35	54	67	98	117	164	176	185
40 mH	5	19	32	51	61	93	114	163	177	183
50 mH	Inf	2	11	28	41	74	94	146	161	163

Table 6
Comparison of the proposed method with recently proposed approaches.

	Fault location method	Power technology	Type of fault	Load	Distribution line length	Remarks	Error (%)
[15]	Current, voltage and arc model parameter estimates at each probable location	AC 24.9 kV – 60 Hz	Parallel high impedance fault	Resistor + inductor	10 – 55 km	Complex calculation in parameters estimation	0.17 – 9.25
[30]	Impedance parameters + Genetic algorithm	28 V	Intermittent parallel arc fault	Resistor	24.6 m	Complex calculation in the solution of equations	—
[35]	Traveling waves (pulses captured by capacitors)	DC 360 V	Series arc fault	Resistor	300 m	Very high synchronization is required	2.5
[36]	Impedance parameters	DC 720 V	Series arc fault	Resistor	1200 m	Selection of a frequency band is required	—
[37]	Impedance parameters	AC 230 V – 50 Hz	Series arc fault	Resistor	49 m	Selection of a frequency band is required	—
[38]	Impedance parameters + Neural Network	AC 230 V – 50 Hz	Series arc fault	Resistor	39 m – 150 m	Sensitive to arc fault impedance variations	6
Proposed method	Impedance parameters	AC 230 V – 50 Hz	Series arc fault	Resistor + inductor	30 m – 190 m	Non sensitive to arc fault impedance variations	1

7. Conclusion

In this study, we have presented a new method for locating series-arc faults, that is based on the virtual capacitive decoupling of a power line. By generating a fault-map trace, obtained at different arc-fault locations, we have enabled the creation of a baseline of main reference points. The fault distance can be calculated by referring to the intersection of the coefficients of the fault map trace and the coefficients, generated by subtracting the estimated currents. This method is also able to estimate fault distances precisely, when studying different line lengths, different line models, as well as different inductance-load values. In addition to this, the results show that this method functions correctly when analyzing electrical-arc faults initiated by either opening contacts or carbonized paths. In this work, the feasibility analysis of the location method is tested on a particular electrical network composed on a single line to be protect. For a complex network with lateral branches, the task is more difficult and has not been tested in this work. In this case, it will probably be necessary to place a locating device at each branch of the line. In conclusion, we can confidently announce that this fault-location method, based on the decoupling of mutual capacitance, shows promising results. Furthermore, it can be used with an embedded electronic card in a manner that is computationally inexpensive.

Declaration of Competing Interest

The authors declare that they have no known competing financial interests or personal relationships that could have appeared to influence the work reported in this paper.

References

[1] FEMA 2008. Topical Fire report series: Residential building electrical Fires. In: United States Fire Administration 8.2; Mar. 2008.
[2] Lee DA, Trotta AM, King WH. New technology for preventing residential electrical fires: Arc-fault. In: Circuit Interrupters (AFCIs). Fire Technol, 36; 2000, p. 146–62.
[3] Dvorak RF, Wong KB. Arc fault circuit interrupter system. Underwriters Laboratories 2007.
[4] Shi Q, Kanoun O. A new algorithm for wire fault location using time-domain reflectometry. IEEE Sens J 2014;14(4):1171–8.
[5] Wu S, Furse C, Lo C. Noncontact probes for wire fault location with reflectometry. IEEE Sens J 2006;6(6):1716–21.
[6] Smith P, Furse C, Gunther J. Analysis of spread spectrum time domain reflectometry for wire fault location. IEEE Sens J 2005;5(6):1469–78.
[7] Shin YJ, Powers EJ, Choe TS, Hong Chan-Young, Song Eun-Seok, Yook Jong-Gwan, et al. Application of time-frequency domain reflectometry for detection and localization of a fault on a coaxial cable. IEEE Trans Instrum Meas 2005;54(6): 2493–500.
[8] Dashti Rahman, Ghasemi Mohsen, Daisy Mohammad. Fault location in power distribution network with presence of distributed generation resources using impedance based method and applying n line model. Energy 2018;159:344–60.
[9] Pustulka M, Izykowski J, Lukowicz M. Comparison of different approaches to arc fault location on power transmission lines. In: 2013 12th International conference on environment and electrical engineering; May 2013. p. 145–9.
[10] Iurinic LU, Herrera-Orozco AR, Ferraz RG, Bretas AS. Distribution systems high-impedance fault location: a parameter estimation approach. IEEE Trans Power Deliv 2016;31(4):1806–14.
[11] Das S, Santoso S, Gaikwad A, Patel M. Impedance-based fault location in transmission networks: theory and application. IEEE Access 2014;2:537–57.
[12] Johns AT, Jamali S. Accurate fault location technique for power transmission lines. IEE Proc C - Gener, Transmiss Distrib 1990;137(6):395–402.
[13] Ferraz Renato G, Iurinic Leonardo U, Filomena Andre D, Gazzana Daniel S, Bretas Arturo S. Arc fault location: A nonlinear time varying fault model and frequency domain parameter estimation approach. Int J Electr Power Energy Syst 2016;80:347–55.
[14] Daisy Mohammad, Dashti Rahman, Shaker Hamid Reza. A new fault-location method for HVDC transmission-line based on DC components of voltage and current under line parameter uncertainty. Electr Eng 2017;99:573–82.
[15] Mortazavi SH, Moravej Z, Shahrtash SM. A searching based method for locating high impedance arcing fault in distribution networks. IEEE Trans Power Deliv 2019;34(2):438–47.
[16] Borghetti A, Corsi S, Nucci CA, Paolone M, Peretto L, Tinarelli R. On the use of continuous-wavelet transform for fault location in distribution power networks. In: 2005 15th Power systems computation conference (PSCC); 2005. p. 1–7.
[17] Shaik Abdul Gafoor, Pulipaka Ramana Rao V. A new wavelet based fault detection, classification and location in transmission lines. Int J Electr Power Energy Syst 2015;64:35–40.
[18] Baseer MA. Travelling waves for finding the fault location in transmission lines. J Electr Electron Eng 2013;1(1):1–19.
[19] Magnago FH, Abur A. Fault location using wavelets. IEEE Trans Power Deliv 1998; 13(4):1475–80.
[20] An Jianwei, Zhuang Chijie, Rachidi Farhad, Zeng Rong. A new fault-location method for HVDC transmission line based on DC components of voltage and current under line parameter uncertainty; 2020. arXiv: 2002.06316 [eess. SP].
[21] Codino A, Wang Z, Razzaghi R, Paolone M, Rachidi F. An alternative method for locating faults in transmission line networks based on time reversal. IEEE Trans Electromagn Compat 2017;59(5):1601–12.
[22] Razzaghi R, Lugrin G, Mahmoudimanesh H, Romero C, Paolone M, Rachidi F. An efficient method based on the electromagnetic time reversal to locate faults in power networks. In: 2014 IEEE PES General Meeting I conference exposition; July 2014. p. 1–1.
[23] El-Naggar KM. A genetic based fault location algorithm for transmission lines. In: 16th International conference and exhibition on electricity distribution, 2001. Part 1: Contributions. CIRED. (IEE Conf. Publ No. 482). Vol. 3; June 2001. 5 pp. vol 3-.
[24] Salat R, Osowski S. Accurate fault location in the power transmission line using support vector machine approach. IEEE Trans Power Syst 2004;19(2):979–86.
[25] Jain Anamika. Artificial neural network-based fault distance locator for double-circuit transmission lines. Adv Artif Intell 2013:1–12.
[26] Alexandre P, da Silva Alves, Lima Antonio CS, Souza Suzana M. Fault location on transmission lines using complex-domain neural networks. Int J Electr Power Energy Syst 2012;43(1):720–7.
[27] Jamil Majid, Kalam Abul, Ansari AQ, Rizwan M. Generalized neural network and wavelet transform based approach for fault location estimation of a transmission line. Appl Soft Comput 2014;19:322–32.
[28] Shafiullah M, Abido MA, Al-Hamouz Z. Wavelet-based extreme learning machine for distribution grid fault location. IET Gener, Transmiss Distrib 2017;11(17): 4256–63.
[29] Perez R, Vasquez C, Viloria A. An intelligent strategy for faults location in distribution networks with distributed generation. J Intell Fuzzy Syst 2019;36(2): 1627–37.
[30] Yaramasu A, Cao Y, Liu G, Wu B. Aircraft electric system intermittent arc fault detection and location. IEEE Trans Aerosp Electron Syst 2015;51(1):40–51.

[31] Moreno R, Arauz P, Kao I. Location and diagnosis of electrical faults for a low-voltage system. In: 2013 15th Recent advances in telecommunications signals and systems conference (PSCC); 2013. p. 157–62.
[32] Karmacharya IM, Gokaraju R. Fault location in ungrounded photovoltaic system using wavelets and ANN. IEEE Trans Power Deliv 2018;33(2):549–59.
[33] Liu X. A Series Arc Fault Location Method for DC Distribution System Using Time Lag of Parallel Capacitor Current Pulses. In: 2018 IEEE international power modulator and high voltage conference (IPMHVC); 2018. p. 218–22.
[34] Xiong Qing, Ji Shengchang, Liu Xiaojun, Feng Xianyong, Zhang Fan, Zhu Lingyu, Gattozzi Angelo L, Hebner Robert E. Detecting and localizing series arc fault in photovoltaic systems based on time and frequency characteristics of capacitor current. Sol Energy 2018;170:788–99.
[35] Xiong Q, Feng X, Gattozzi AL, Liu X, Zheng L, Zhu L, Ji S, Hebner RE. Series arc fault detection and localization in DC Distribution System. IEEE Trans Instrum Meas 2020;69(1):122–34.
[36] Cao Y, Li J, Sumner M, Christopher E, Thomas DWP. A new double-ended approach to the series arc fault location. In: 12th IET International conference on developments in power system protection (DPSP 2014); Mar. 2014. p. 1–5.
[37] Calderon EM, Schweitzer P, Weber S. A series arc fault location algorithm based on an impedance method for a domestic AC system. In: 2017 IEEE Holm conference on electrical contacts; Sept. 2017. p. 312–6.
[38] Calderon-Mendoza E, Schweitzer P, Weber S. A double ended AC series arc fault location algorithm for a low-voltage indoor power line using impedance parameters and a neural network. Electric Power Syst Res 2018;165:84–93.
[39] Lezama J, Schweitzer P, Weber S, Tisserand E, Joyeux P. Modeling of a Domestic Electrical Installation to Arc Fault Detection. In: 2012 IEEE 58th Holm conference on electrical contacts (Holm); Sept. 2012. p. 1–7.
[40] Andrea J, Schweitzer P, Carvou E. Comparison of Equations of the VI Characteristics of an Electric Arc in Open Air. In: 2019 IEEE Holm Conference on Electrical Contacts; Sept. 2019. p. 76–81.
[41] Andrea J, Schweitzer P, Martel J. Arc fault model of conductance. Application to the UL1699 Tests Modeling. In: 2011 IEEE 57th Holm Conference on Electrical Contacts (Holm); Sept. 2011. p. 1-6.